The Electronic Structures of Co and Ni Tetraazaannulenes

Jing Liu,[†] Jie Xiao,[†] Seok-Bong Choi,[‡] P. Jeppson,[†,‡] L. Jarabek,[‡] Ya. B. Losovyj,[§] A. N. Caruso,*[,‡] and P. A. Dowben*[,†]

Department of Physics and Astronomy and the Nebraska Center for Materials and Nanoscience, Behlen Laboratory of Physics, University of Nebraska-Lincoln, Lincoln, Nebraska, 68588-0111, Center for Nanoscale Science and Engineering, North Dakota State University, Fargo, North Dakota, 58102, and Center for Advanced Microstructures and Devices, Louisiana State University, 6980 Jefferson Highway, Baton Rouge, Louisiana 70806

Received: August 29, 2006; In Final Form: October 4, 2006

We compare the electronic structure of two metal-centered tetramethyldibenzo−tetraazaannulene (TMTAA) macrocyclic complex molecules: 5,7,12,14- tetramethyl-2,3:9,10-dibenzo[b,i]-1,4,8,11-tetraazacyclotetradecine nickel (II) and 5,7,12,14-tetramethyl-2,3:9,10-dibenzo[b,i]-1,4,8,11-tetraazacyclotetradecine cobalt (II). The experimental gap between the highest occupied molecular orbital to the lowest unoccupied molecular orbital for both molecules, obtained from combined ultraviolet photoemission and inverse photoemission studies, is close to the value of 6.6 eV expected from simple model calculations, but with the Fermi level placed closer to the lowest unoccupied molecular orbital. While both the Co(II) ($s = 1/2$) and Ni(II) ($s = 0$) TMTAA molecular electronic structures are very similar, the Ni(II) adopts a high-symmetry molecular configuration upon adsorption, with a strong preferential orientation.

Introduction

The macrocycle metalloporphyrins and their metal complexes such as tetraazaannulene (TAA) have been extensively studied by Raman, infrared, and other vibration spectroscopies[1−5] but, unlike the metal phthalocyanines,[6−14] the electronic structure of the metal TAA species has not been given much attention. This is surprising given that a number of different transition metal substitutions are possible, as is seen to be the case for the 3d transition metal metallocenes. Such comparisons are important because it now seems clear that adsorbed cobaltocene[15] is far less stable as a molecule on surfaces than ferrocene[16−25] ($Z - 1$) or nickelocene[25−30] ($Z + 1$). The big difference among these three metallocenes appears to be that the 19-electron cobaltocene has a single unpaired electron, resulting in a low ionization potential[31] of 5.56 eV[32] when compared to that of ferrocene (6.88 eV[32]) and nickelocene (6.51 eV[32]).

Does the unpaired electron similarly affect the electronic structure and preferential orientation of adsorbed 5,7,12,14-tetramethyl-2,3:9,10-dibenzo[b,i]-1,4,8,11-tetraazacyclotetradecine cobalt (II) (Co(II)TMTAA) with respect to 5,7,12,14-tetramethyl-2,3:9,10-dibenzo[b,i]-1,4,8,11-tetraazacyclotetradecine nickel (II) (Ni(II)TMTAA)? Although often regarded as planar, the metal-centered tetramethyldibenzo−tetraazaannulene (TMTAA) macrocyclic complex molecules are, in fact, saddle shaped,[33] as indicated in the schematic structures shown in Figure 1, because the negative charge of $TMTAA^{2-}$ is localized on the nitrogen atoms rather than the entire framework. The saddle-shaped structure of the free molecule may be readily altered upon adsorption onto a solid metal surface. Molecular adsorption results in a change in the charge distribution near the surface[13,14,34] and can alter the molecular electric dipole along the surface normal.[6,34] Thus, the expectation is that differences should be seen in the electronic structure between the various adsorbed metal-centered TMTAA macrocyclic complex molecules, differing only in the central metal atom.

Experiment and Theory

The complexes Co(II)TMTAA[35] and Ni(II)TMTAA[36] were synthesized according to a modified procedure, and their structures were confirmed by elemental analysis and Fourier transform infrared and NMR spectroscopies.

The occupied and unoccupied electronic structure of the absorbed Co(II)TMTAA and Ni(II)TMTAA molecular films on Au(111) were studied by ultraviolet photoemission spectroscopy (UPS) and inverse photoemission spectroscopy (IPES), respectively. The Au(111)-coated silicon substrates were cleaned by argon ion sputtering and verified by X-ray photoelectron spectroscopy before each adsorption. The adsorbed molecular thin films were prepared by adsorption from vapor on clean gold, cooled to the vicinity of 170 K (to suppress fragmentation and improve resolution). Both the Co(II)TMTAA and Ni(II)-TMTAA vapors were introduced into an ultrahigh vacuum (UHV) chamber through a standard leak valve. From UPS and IPES spectra of Co(II)TMTAA and Ni(II)TMTAA, we can see that the Au(111) substrate features are completely suppressed, which indicates that the thickness of these molecular films exceeded the mean free path of photoelectrons from the substrate Au(111) (>3 nm thick).

Angle-resolved photoemission (ARPES) experiments were carried out using a photon energy of 55 eV, dispersed by a 3 m

* To whom correspondence should be addressed. Peter Dowben, Department of Physics and Astronomy and the Nebraska Center for Materials and Nanoscience, Behlen Laboratory of Physics, University of Nebraska, Lincoln, Nebraska 68588-0111; tel.: 402-472-9838; fax: 402-472-2879; e-mail: pdowben@unl.edu. Anthony Caruso, Center for Nanoscale Science and Engineering, North Dakota State University, Fargo, ND 58102; tel.: 701-231−5816; e-mail: anthony.caruso@ndsu.edu.

[†] University of Nebraska-Lincoln.

[‡] North Dakota State University.

[§] Louisiana State University.

10.1021/jp0656126 CCC: $33.50
Published on Web 11/23/2006

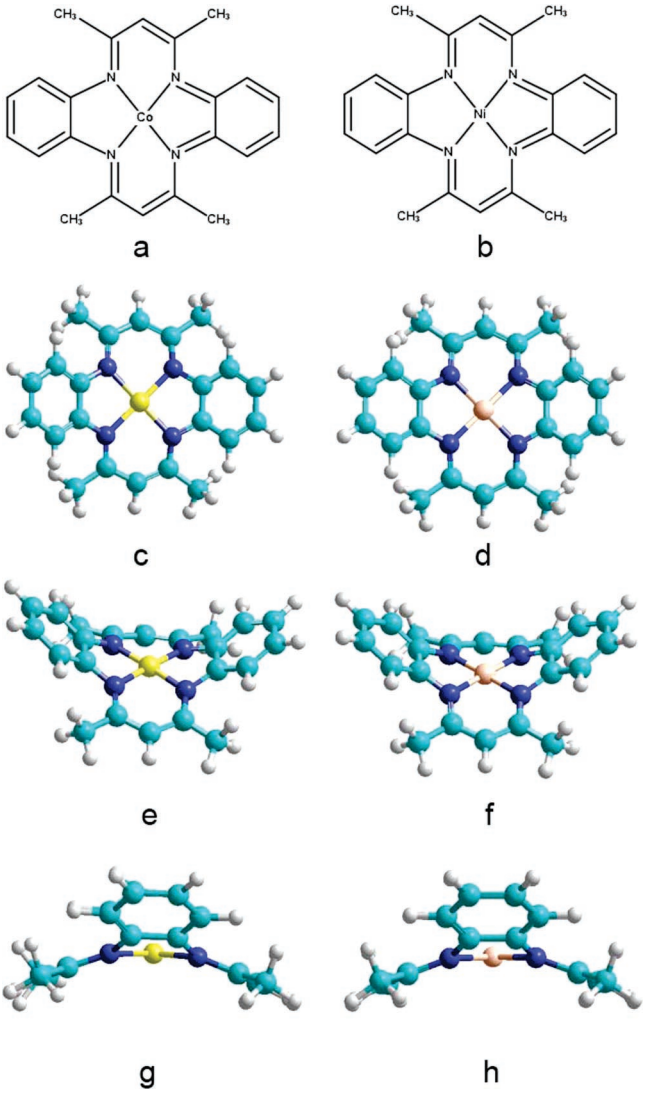

Figure 1. The chemical structure of Co(II)TMTAA (a) and Ni(II)-TMTAA (b) molecules, along with the geometry optimized structures viewed from the top (Co(II)TMTAA (c) and Ni(II)TMTAA (d)) and from two side views (Co(II)TMTAA (e,g) and Ni(II)TMTAA (f,h)).

toroidal monochromator at the Center for Advanced Microstructures and Devices synchrotron facility in Baton Rouge, Louisiana, as described in detail elsewhere.[15,18,37−38] The measurements were performed in a UHV chamber employing a hemispherical electron energy analyzer with an angular acceptance of ±1°, with photoelectrons collected normal to the surface. The combined resolution of the electron energy analyzer and the monochromator is about 150 meV for the measurement undertaken here. All angles (both light incidence angles as well as photoelectron emission angles) reported herein are with respect to the substrate surface normal. A comparison of the photoemission spectra taken with ***E*** residing equally in the surface plane and surface normal (a light incidence angle of 45° off the surface normal) with that of ***E*** being more parallel to the surface normal (a light incidence angle of 60° off the surface normal) was used to probe a preferential molecular orientation. The light polarization dependence of the photoemission signal, related to a particular feature in the spectra, is based on the photoemission selection rules and is closely related to the specific symmetry of involved molecular orbitals.[7,15,17,18,20,23,24,38] For the photoemission results reported here, the photoelectrons were collected normal to the substrate surface (i.e., $k_{||} = 0$ or $\bar{\Gamma}$) to preserve the highest possible local point group symmetry. For example, this means that the application of symmetry selection rules to a molecular system with a C_{2v} point group symmetry, with the high symmetry axis along the surface normal, causes the molecular orbitals of a_1 symmetry to become enhanced with ***E*** residing more along the surface normal, whereas b_1 and b_2 symmetry molecular orbitals are enhanced with ***E*** residing more in the plane of the surface.

The IPES studies were performed by using a variable-energy electron gun producing electron kinetic energies from 5 to 19 eV, incident normal to surface. An I_2/He Geiger−Müller detector with a CaF_2 window, positioned at 45° off the surface normal, was used to measure the emitted photons at a fixed energy (9.7 eV), with an overall inverse photoemission resolution of ~400 meV, as described elsewhere.[38−39] All binding energies are referenced with respect to the Fermi level ($E - E_F$) determined from spectra taken of both clean gold and tantalum in intimate contact with the sample surface for both photoemission and inverse photoemission.

The semiempirical theoretical calculations were undertaken to model the Co(II)TMTAA and Ni(II)TMTAA molecular structures by PM3 (neglect of differential overlap, parametric method 3)[40−41] with the HyperChem package. Geometric optimization of the system was performed obtaining the lowest unrestricted Hartree−Fock energy states and their possible symmetries: the structures of Co(II)TMTAA and Ni(II)TMTAA molecules are shown in Figure 1. The geometry optimized structures of both molecules (Figure 1c−f), from these model calculations resulted in a typical saddle-shaped conformation, consistent with the previous reports of metal-centered TMTAA and other ion complexes.[33,42]

Although our ground-state calculations are hardly ideal, like similar semiempirical molecular orbitals calculations (NNDO, MNDO, INDO, CNDO), our simple molecular orbital calculations have successfully recovered much of the detail observed in large molecular systems using photoemission and inverse photoemission, including reproducing, with reasonable agreement, the highest occupied molecular orbital (HOMO) to lowest unoccupied molecular orbital (LUMO) gap.[18,23,24,26,43] In spite of the severe limitations of these simple molecular orbital calculations, they can be compared, with some effect, to conventional density functional theory calculations.[44]

The HOMO−LUMO Gap

With the thicker molecular films, where contributions from the substrate are suppressed, we can use the combination of photoemission and inverse photoemission to estimate the HOMO−LUMO gap, as well as ascertain the relative molecular orbital contributions to the density of states (DOS), with the assistance of theory (although one should acknowledge that such a comparison is undertaken with a number of caveats and limitations, as noted above). This has been done for both Co(II)TMTAA (Figure 2) and Ni(II)TMTAA (Figure 3).

The expected HOMO−LUMO agrees well with the value obtained from the combined photoemission and inverse photoemission studies. The energy gap between the HOMO and LUMO can be derived from the combined photoemission and inverse photoemission spectra (Figures 2 and 3). The experimental HOMO−LUMO gap is 6.5 ± 0.3 eV for Co(II)TMTAA, which is in excellent agreement with the theoretical estimate of the HOMO−LUMO gap of 6.6 eV. For Ni(II)TMTAA, the experimental HOMO−LUMO gap is 6.8 ± 0.4 eV, which is also in excellent agreement with the theoretical value of the HOMO−LUMO gap (again 6.6 eV).

The combined photoemission and inverse photoemission spectra (Figures 2 and 3 of Co(II)TMTAA and Ni(II)TMTAA,

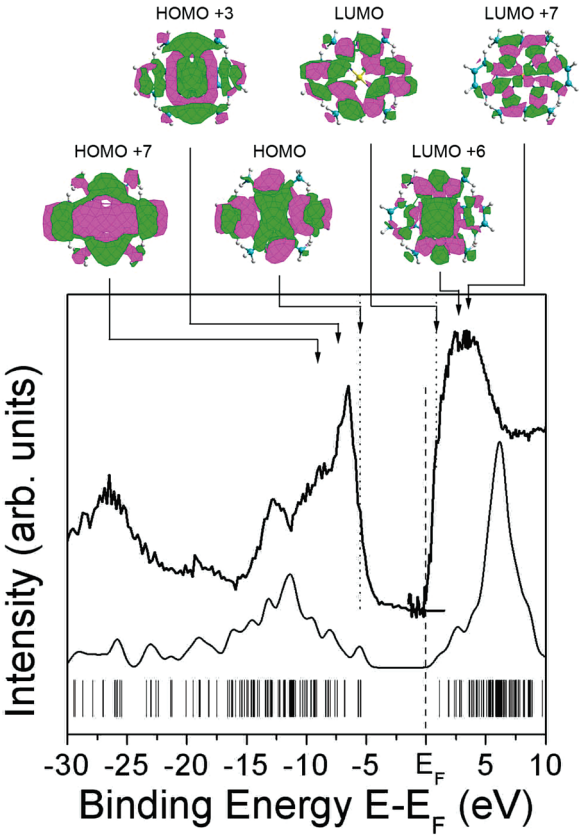

Figure 2. Combined UPS (left) and IPES (right) spectra (top curve) of Co(II)TMTAA, highlighting the experimental band gap, with the calculated molecular orbitals (bottom black lines) and model DOS, without any corrections for matrix element or cross-section effects (middle curve). Schematics of the charge density distributions of the HOMO, HOMO+3, HOMO+7, LUMO, LUMO+6 and LUMO+7 are presented in the inset.

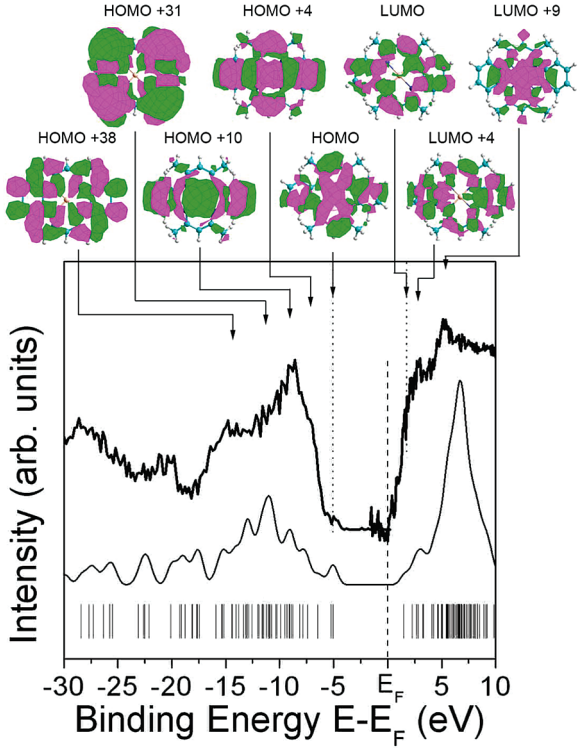

Figure 3. Combined UPS (left) and IPES (right) spectra (top curve) of Ni(II)TMTAA, highlighting the experimental band gap, with the calculated molecular orbital energies (bottom black lines) and model DOS, without any corrections for matrix element or cross-section effects (middle curve). Schematics of the charge density distributions of the HOMO, HOMO+4, HOMO+10, HOMO+31, HOMO+38, LUMO, LUMO+4 and LUMO+9 are presented in the inset.

respectively) indicate that both metal TAA species are n-type molecular films, as a result of the Fermi level sitting closer to the LUMO band edge than the HOMO band edge. While we cannot directly identify the majority carriers from the photoemission and inverse photoemission, the close proximity of the Fermi level to the experimental LUMO band edge may be one reason why many macrocycle metalloporphyrins are conductors, in spite of the relatively large HOMO−LUMO gaps (in this case, 6.5−6.8 eV). Thus, the effective transport gap[8] may, in fact, be quite small.

The Metal TAA Electronic Structure

The calculated electronic structures for Co(II)TMTAA and Ni(II)TMTAA are very similar. A calculated DOS was obtained by applying equal Gaussian envelopes of 1 eV full width half-maximum to each molecular orbital (to account for the solid-state broadening in photoemission) and summing. This calculated DOS, when combined with a rigid energy shift of 2.1 eV for Co(II)TMTAA and 2.4 eV for Ni(II)TMTAA applied to the calculated electronic structure, qualitatively aligns with the features seen in the combined photoemission and inverse photoemission data, as seen in Figures 2 and 3. There are profound differences in the molecular orbital peak intensities between experiment and theory, however, as seen in Figures 2 and 3.

The model calculations do not account for photoemission and inverse photoemission matrix element effects, thus the comparison to photoemission and inverse photoemission must be considered only qualitatively. Some molecular orbitals with strong 3d cobalt weight are seen to have much stronger photoemission intensities than expected from the model calculations, particularly for the molecular orbitals close to the HOMO and LUMO molecular orbitals, as identified in the photoemission and inverse photoemission spectra (Figures 2 and 3). The strong photoemission feature of Co(II)TMTAA at −5.6 eV ($E - E_F$) originates from molecular orbitals of strong 3d cobalt weight, while the 3d state of nickel contributes to the Ni(II)TMTAA photoemission features at −5.6 and −7.4 eV ($E - E_F$). This is partly indicated by the schematic molecular orbital diagrams in Figures 2 and 3, associated with some of the photoemission and inverse photoemission features.

In spite of the deficiencies of the model calculations and some differences in both the photoemission and inverse photoemission of Co(II)TMTAA and Ni(II)TMTAA, the electronic structures of these two molecules are very similar, as are the HOMO−LUMO gaps. The ligand field splitting of the metal d-band weighted molecular orbitals is seen to result in a better definition of these features in both photoemission and inverse photoemission from Ni(II)TMTAA (Figure 3) than for Co(II)TMTAA (Figure 2). Although not compelling, this suggests that the point group symmetry of adsorbed Ni(II)TMTAA is higher than that for Co(II)TMTAA. Adopting a higher point group symmetry would result in a lifting of degenerate and nearly degenerate molecular orbitals. The surmise that adsorbed Ni(II)TMTAA is in a higher point group symmetry than Co(II)TMTAA is, in fact, supported by the angle-resolved light polarization-dependent photoemission.

Preferential Bonding Orientation for Ni(II)TMTAA

On the basis of these semiempirical PM3 calculations, we can ascertain the nominal symmetries of the molecular orbitals

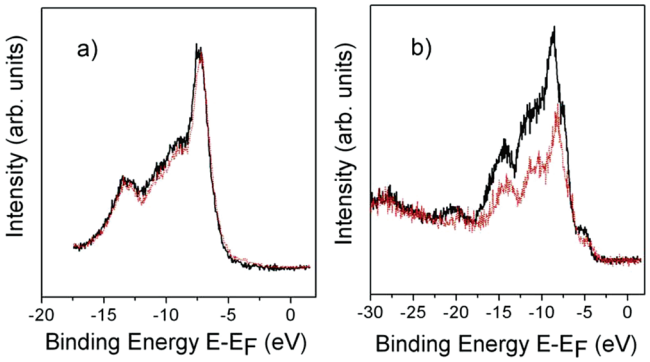

Figure 4. Comparison of the ARPES spectra of Co(II)TMTAA (a) and Ni(II)TMTAA (b) taken with ***E***, of the incident polarized light, residing more along the surface normal (black) and with ***E*** residing more in the plane of the surface (red). The spectra were taken at a photon energy of 55 eV. The photoelectrons were collected at normal emission.

that contribute to the various photoemission and inverse photoemission features, as indicated in Figures 2 and 3. Because of the expected saddle-shaped structures of Co(II)TMTAA and Ni(II)TMTAA mentioned above, we expected that the ARPES spectra of Co(II)TMTAA and Ni(II)TMTAA should show little evidence of symmetry and selection rules in photoemission. The absence of evidence of symmetry in photoemission, however, can indicate a lack of preferential orientation or a low point group molecular symmetry for the molecular adsorbate. This clarification is important because the light polarization-dependent photoemission of adsorbed Co(II)TMTAA on Au(111) is very different from that of Ni(II)TMTAA on Au(111), as seen in Figure 4.

The absence of symmetry selection rule effects means that, as expected, there is little dependence of the photoemission spectra upon the polarization of the incident light for absorbed Co(II)TMTAA on Au(111), as seen in Figure 4a. For absorbed Ni(II)TMTAA (Figure 4b), there are clear enhancements of the photoemission features attributable to the HOMO+2 through HOMO+48 orbitals, with ***E*** residing more along the surface normal. While this does not actually suggest that photoemission is enhanced for all molecular orbitals between the HOMO+2 through HOMO+48 orbitals, the light polarization-dependent photoemission does suggest a strong dipole along the surface normal and that Ni(II)TMTAA may well adopt a C_{2v} symmetry with the molecular axis along the surface normal and the molecular plane parallel with the surface. The Ni(II)TMTAA adopts a high group symmetry with respect to the surface normal upon adsorption (and becomes quite flat), while Co(II)TMTAA does not.

The lower symmetry realized by adsorbed Co(II)TMTAA relative to Ni(II)TMTAA may also be the origin of the significantly greater cross-section for Co(II)TMTAA inverse photoemission and a different conduction band edge structure. The experimental cross-section of adsorbed Co(II)TMTAA is nearly twice as large as that of adsorbed Ni(II)TMTAA. The cross-section depends on the initial state (whose parity is always even in inverse photoemission), so the larger currents measured for Co(II)TMTAA in inverse photoemission experiments suggest not only a greater cross-section but also that fewer selection rules apply. In Figure 2, The differences between the model calculations and experimental data for Co(II)TMTAA also suggest that the selection rules for absorbed Co(II)TMTAA are altered, and the matrix element effects are different.

The greater symmetry and the much larger preferential orientation combined with the better definition for the 3d metal weighted molecular orbitals for Ni(II)TMTAA suggest that this metal TAA almost certainly adopts a singlet state upon adsorption, resulting in greater molecular symmetry. The metal TAA Co(II)TMTAA does not appear to favor a greater symmetry, or fails to adopt a preferential orientation upon adsorption on Au(111). Although this is speculative at this point, it may be that for Co(II)TMTAA, like adsorbed cobaltocene[15] and gaseous CF_4^+,[45] the unpaired spin not only results in the adoption of a lower point group symmetry but also in a much more fragile molecular species.

Conclusions

The experimental HOMO−LUMO gaps for Co(II)TMTAA (6.5 eV ± 0.3 eV) and Ni(II)TMTAA (6.8 eV ± 0.4 eV) are generally in good agreement with expectations (6.6 eV), and there is clearly some correspondence between the experimental electronic structure and simple model calculations, although the model calculations do not accurately reproduce the observed partial photoemission and inverse photoemission cross-sections. The location of the Fermi level suggests that both absorbed metal-centered TMTAAs are n-type insulators on Au(111) substrates.

Acknowledgment. This work was supported by the National Science Foundation through grant CHE-0415421, ND EPSCoR grant EPS-0447679, and the NSF "QSPINS" MRSEC (DMR 0213808), as well as the Defense Microelectronics Activity (DMEA) under agreement DMEA90-02-2-0218. The authors also wish to thank the Center for Advanced Microstructures and Devices, which is funded by the State of Louisiana.

References and Notes

(1) Woodruff, W. H.; Pastor, R. W.; Dabrowiak, J. C. *J. Am. Chem. Soc.* **1976**, *98*, 7999.

(2) Nafie, L. A.; Pastor, R. W.; Dabrowiak, J. C.; Woodruff, W. H. *J. Am. Chem. Soc.* **1976**, *98*, 8007.

(3) Bell, S.; Crayston, J. A.; Dines, T. J.; Ellahi, S. B.; Smith, C. I. *Inorg. Chem.* **2003**, *42*, 3565.

(4) Bell, S.; Crayston, J. A.; Dines, T. J.; Ellahi, S. B. *J. Phys. Chem.* **1996**, *100*, 5252.

(5) Reddy, K. H.; Reddy, M. R.; Raju, K. M. *Polyhedron* **1997**, *16*, 2673.

(6) Fukagawa, H.; Yamane, H.; Kera, S.; Okudaira, K. K.; Ueno, N. *Phys. Rev. B* **2006**, *73*, 041302(R). Yamane, H.; Yabuuchi, Y.; Fukagawa, H.; Kera, S.; Okudaira, K. K.; Ueno, N. *J. Appl. Phys.* **2006**, *99*, 093705.

(7) Permien, T.; Engelhardt, R.; Feldman, C. A.; Koch, E. E. *Chem. Phys. Lett.* **1983**, *98*, 527. Richardson, N. V. *Chem. Phys. Lett.* **1983**, *102*, 390.

(8) Zahn, D. R. T.; Gavrila, G. N.; Gorgoi, M. *Chem. Phys.* **2006**, *325*, 99.

(9) Ueno, N.; Suzuki, K.; Hasegawa, S.; Kamiya, K.; Seki, K.; Inokuchi, H. *J. Chem. Phys.* **1993**, *99*, 7169. Okudaira, K. K.; Hasegawa, S.; Ishii, H.; Seki, K.; Harada, Y.; Ueno, N. *J. Appl. Phys.* **1999**, *85*, 6453.

(10) Ueno, N.; Kamiya, K.; Ogawa, K.; Yonehara, H.; Takahashi, M.; Nakahara, H.; Seki, K.; Sugita, K.; Fukuda, K.; Inokuchi, H. *Thin Solid Films* **1992**, *210/211*, 678.

(11) Aoki, M.; Masuda, S.; Einaga, Y.; Kamiya, K.; Kitamura, A.; Momose, M.; Ueno, N.; Harada, Y.; Miyazaki, T.; Hasegawa, S.; Inokuchi, H.; Seki, K. *J. Electron Spectrosc. Rel. Phenom.* **1996**, *76*, 259.

(12) Kera, S.; Abduaini, A.; Aoki, M.; Okudaira, K. K.; Ueno, N.; Harada, Y.; Shirota, Y.; Tsuzuki, T. *Thin Solid Films* **1998**, *278*, 327. Kera, S.; Abduaini, A.; Aoki, M.; Okudaira, K. K.; Ueno, N.; Harada, Y.; Shirota, Y.; Tsuzuki, T. *J. Electron Spectrosc. Relat. Phenom.* **1998**, *885*, 88. Kera, S.; Yamane, H.; Sakuragi, I.; Okudaira, K. K.; Ueno, N. *Chem. Phys. Lett.* **2002**, *364*, 93.

(13) Yamane, H.; Fukagawa, H.; Honda, H.; Kera, S.; Okudaira, K. K.; Ueno, N. *Synth. Met.* **2005**, *152* (Part 1 Spec. Iss. SI), 297. Kera, S.; Yamane, H.; Honda, H.; Fukagawa, H.; Okudaira, K. K.; Ueno, N. *Surf. Sci.* **2004**, *566*; 571. Munakata, T.; Sugiyama, T.; Masuda, T.; Aida, M.; Ueno, N. *Appl. Phys. Lett.* **2004**, *85*, 3584.

(14) Fukagawa, H.; Yamane, H.; Kera, S.; Okudaira, K. K.; Ueno, N. *J. Electron Spectrosc. Relat. Phenom.* **2005**, *144*, 475. Kera, S.; Yabuuchi, Y.; Yamane, H.; Setoyama, H.; Okudaira, K. K.; Kahn, A.; Ueno, N. *Phys.*

Rev. B **2004**, *70*, 085304. Yamane, H.; Honda, H.; Fukagawa, H.; Ohyama, M.; Hinuma, Y.; Kera, S.; Okudaira, K. K.; Ueno, N. *J. Electron Spectrosc. Relat. Phenom.* **2004**, *137*, 223. Schwieger, T.; Peisert, H.; Knupfer, M. *Chem. Phys. Lett.* **2004**, *384*, 197. Gorgoi, M.; Zahn, D. R. T. *Appl. Surf. Sci.* **2006**, *252*, 5453. Peisert, H.; Knupfer, M.; Zhang, F.; Petr, A.; Dunsch, L.; Fink, J. *Surf. Sci.* **2004**, *566*, 554.

(15) (15) Choi, J.; Dowben, P. A. *Surf. Sci.* **2006**, *600*, 2997.

(16) Welipitiya, D.; Green, A.; Woods, J. P.; Dowben, P. A.; Robertson, B. W.; Byun, D.; Zhang, J. *J. Appl. Phys.* **1996**, *79*, 8730.

(17) Welipitiya, D.; Dowben, P. A.; Zhang, J.; Pai, W. W.; Wendelken, J. F. *Surf. Sci.* **1996**, *367*, 20.

(18) Waldfried, C.; Welipitiya, D.; Hutchings, C. W.; de Silva, H. S. V.; Gallup, G. A.; Dowben, P. A.; Pai, W. W.; Zhang, J.; Wendelken, J. F.; Boag, N. M. *J. Phys. Chem. B* **1997**, *101*, 9782.

(19) Durston, P. J.; Palmer, R. E. *Surf. Sci.* **1998**, *400*, 277.

(20) Dowben, P. A.; Waldfried, C.; Komesu, T.; Welipitiya, D.; McAvoy, T.; Vescovo, E. *Chem. Phys. Lett.* **1998**, *283*, 44.

(21) Svensson, K.; Bedson, T. R.; Palmer, R. E. *Surf. Sci.* **2000**, *451*, 250.

(22) Woodbridge, C. M.; Pugmire, D. L.; Johnson, R. C.; Boag, N. M.; Langell, M. A. *J. Phys. Chem. B* **2000**, *104*, 3085.

(23) Dowben, P. A. *Z. Phys. Chem.* **1997**, *202*, 227.

(24) Dowben, P. A.; Choi, J.; Morikawa, E.; Xu, B. The Band Structure and Orientation of Molecular Adsorbates on Surfaces by Angle-Resolved Electron Spectroscopies. In *Characterization and Spectroscopy of Thin Films*; Nalwa, H. S., Ed.; Handbook of Thin Films; Academic Press: New York, 2002; Vol. 2, Chapter 2, pp 61−114.

(25) Zanoni, R.; Piancastelli, M. N.; Marsi, M.; Margaritondo, G. *J. Electron Spectrosc. Relat. Phenom.* **1991**, *57*, 199.

(26) Welipitiya, D.; Borca, C. N.; Waldfried, C.; Hutchings, C.; Sage, L.; Woodbridge, C. M.; Dowben, P. A. *Surf. Sci.* **1997**, *393*, 34.

(27) Pugmire, D. L.; Woodbridge, C. M.; Langell, M. A. *Surf. Sci.* **1998**, *411*, L844.

(28) Pugmire D. L.; Woodbridge, C. M.; Root, S.; Langell, M. A. *J. Vac. Sci. Technol. A* **1999**, *17*, 1581.

(29) Borca, C. N.; Welipitiya, D.; Dowben, P. A.; Boag, N. M. *J. Phys. Chem. B* **2000**, *104*, 1047.

(30) Pugmire, D. L.; Woodbridge, C. M.; Boag, N. M.; Langell, M. A. *Surf. Sci.* **2001**, *472*, 155.

(31) Henrion, O.; Jaegermann, W. *Surf. Sci.* **1997**, *387*, L1073.

(32) Evans, S.; Green, M. L. H.; Jewitt, B.; King, G. H.; Orchard, A. F. *J. Chem. Soc., Faraday Trans. 2* **1974**, *70*, 356.

(33) Walter, M. D.; Fandos, R.; Andersen, R. A. *New J. Chem.* **2006**, *30*, 1065.

(34) Zhu, X. Y. *Surf. Sci. Rep.* **2004**, *56*, 1. Knupfer, M.; Paasch, G. *J. Vac. Sci. Technol. A* **2005**, *23*, 1072.

(35) L'Eplattenier, F. A.; Pugin, A. *Helv. Chim. Acta* **1975**, *58* (3), 917.

(36) Sakata, K.; Tagami, H.; Hashimoto, M. *J. Heterocycl. Chem.* **1989**, *26*, 805. Place, D. A.; Ferrara, G. P.; Harland, J. J.; Dabrowiak, J. C. *J. Heterocycl. Chem.* **1980**, *17*, 439. Weiss, M. C.; Gordon, G. C.; Goedken, V. L. *J. Am. Chem. Soc.* **1979**, *101*, 857.

(37) Dowben, P. A.; LaGraffe, D.; Onellion, M. *J. Phys.: Condens. Matter* **1989**, *1*, 6571.

(38) Feng, D.-Q.; Caruso, A. N.; Schulz, D.; Losovyj, Ya. B.; Dowben, P. A. *J. Phys. Chem. B* **2005**, *109*, 16382.

(39) McIlroy, D. N.; Waldfried, C.; McAvoy, T.; Choi, J.; Dowben, P. A.; Heskett, D. *Chem. Phys. Lett.* **1997**, *264*, 168.

(40) Stewart, J. J. P. *J. Comput. Chem.* **1989**, *10*, 209. Stewart, J. J. P. *J. Comput. Chem.* **1989**, *10*, 221.

(41) Stone, A. J. *Mol. Phys.* **1980**, *41*, 1339.

(42) Klose, A.; Solari, E.; Floriani, C.; Re, N.; Chiesi-Villa, A.; Rizzoli, C. *Chem. Commun.* **1997**, *23*, 2297. Angelis, S. D.; Solari, E.; Gallo E.; Floriani, C.; Chiesi-Villa, A. *Inorg. Chem.* **1992**, *31*, 2520. Nikonov, G. I.; Blake, A. J.; Mountford, P. *Inorg. Chem.* **1997**, *36*, 1107.

(43) Feng, D.-Q.; Losovyj, Ya. B.; Tai, Y.; Zharnikov, M.; Dowben, P. A. *J. Mater. Chem.* **2006**, *16*, 4343. Ford, W. K.; Duke, C. B.; Paton, A. *J. Chem. Phys.* **1983**, *78*, 4734. Yoshimura, D.; Ishii, H.; Ouchi, Y.; Miyamae, T.; Hasegawa, S.; Okudaira, K. K.; Ueno, N.; Seki, K. *J. Chem. Phys.* **2004**, *120*, 10753. Zojer, E.; Knupfer, M.; Shuai, Z.; Bredas, J. L.; Fink, J.; Leising, G. *J. Phys.: Condens. Matter* **2000**, *12*, 1753. Chambers, D. K.; Karanam, S.; Qi, D.; Selmic, S.; Losovyj, Y. B.; Rosa, L. G.; Dowben, P. A. *Appl. Phys. A* **2005**, *80*, 483. Caruso, A. N.; Feng, D.-Q.; Losovyj, Ya. B.; Shulz, D.; Balaz, S.; Rosa, L. G.; Sokolov, A.; Doudin, B.; Dowben, P. A. *Phys. Status Solidi B* **2006**, *243*, 1321.

(44) Rosa, L. G.; Xiao, J.; Losovyj, Ya. B.; Gao, Y.; Yakovkin, I. N.; Zeng, X. C.; Dowben, P. A. *J. Am. Chem. Soc.* **2005**, *127*, 17261. Park, K.; Pederson, M. R.; Boyer, L. L.; Mei, W. N.; Sabirianov, R. F.; Zeng, X. C.; Bulusu, S.; Curran, S.; Dewald, J.; Day, E.; Adenwalla, S.; Diaz, M.; Rosa, L. G.; Balaz, S.; Dowben, P. A. *Phys. Rev. B* **2006**, *73*, 035109.

(45) Kime, Y. J.; Driscoll, D. C.; Dowben, P. A. *J. Chem. Soc., Faraday Trans. 2* **1987**, *83*, 403. Kime, Y. J.; Dowben, P. A. *J. Phys. Chem.* **1989**, *93*, 6881. Hagenow, G.; Denzer, W.; Brutschy, B.; Baumgärtel, H. *J. Phys. Chem.* **1988**, *92*, 6487. Deutsch, H.; Leiter, K.; Märk, T. D. *Int. J. Mass Spectrom. Ion Processes* **1985**, *67*, 191.